Environmental and Microbial Technology
https://www.sciltp.com/journals/emt

Article

Radiation-Induced Carboxyl-Functionalized Sweet Sorghum Stalk for Adsorption of Cu(II), Zn(II), Pb(II) and Cr(VI)

Jinling Wu [1,2,*], Jing Dong [1] and Xuan Guo [1]

[1] Laboratory of Environmental Technology, INET, Tsinghua University, Beijing 100084, China
[2] Beijing Key Laboratory of Radioactive Waste Treatment, Tsinghua University, Beijing 100084, China
* Correspondence: jinlingwu@tsinghua.edu.cn; Tel.: +86-10-6279-6856

How To Cite: Wu, J.; Dong, J.; Guo, X. Radiation-Induced Carboxyl-Functionalized Sweet Sorghum Stalk for Adsorption of Cu(II), Zn(II), Pb(II) and Cr(VI). *Environmental and Microbial Technology* **2026**, *1*(1), 13. https://doi.org/10.53941/emt.2026.100013

Received: 26 February 2026
Revised: 25 March 2026
Accepted: 21 April 2026
Published: 29 April 2026

Abstract: Heavy metal pollution caused by industrial activities and improper waste disposal poses severe threats to ecosystems and human health, as heavy metal can accumulate in the food chain. Conventional remediation methods are limited by high costs, secondary pollution and poor selectivity for low-concentration heavy metal ions, while agricultural waste-based biosorbents suffer from insufficient active sites and low adsorption capacity. Carboxyl-functionalized sweet sorghum stalk fermentation residue biosorbent FSSR-g-AAm-EDA-SA (FSSR-AES) was synthesized via a two-step modification: Co-60 γ-ray irradiation grafting of acrylamide followed by reaction with ethylenediamine and succinic anhydride. FSSR-AES was characterized by FTIR, SEM-EDS and titration, with carboxyl content reaching 2.55 mmol/g. Static adsorption experiments were carried out under the following conditions: initial metal ion concentrations ranged from 25 to 250 mg/L, prepared with $CuCl_2$, $ZnCl_2$, $PbCl_2$, and $K_2Cr_2O_7$, respectively. The initial pH was adjusted to 6.0 for the adsorption of Cu(II), Zn(II), and Pb(II), and to 2.0 for Cr(VI). The adsorbent dosage was 0.1 g for Cu(II), Zn(II), and Cr(VI) adsorption, while 0.05 g of adsorbent was used for Pb(II) adsorption. Isothermal model fitting showed FSSR-AES achieved maximum adsorption capacities of 21.7, 29.5, 43.1 and 34.9 mg/g for Cu(II), Zn(II), Pb(II) and Cr(VI) at 313.15 K, respectively. Adsorption conformed to the Langmuir model (monolayer chemisorption), with Cu(II) following Freundlich at low temperatures. The higher adsorption of FSSR-AES compared to unmodified FSSR (q_m of 1.9, 6.9 and 23 mg/g for Cu(II), Pb(II) and Cr(VI) under the same operational conditions) is attributed to its high carboxyl group content, which provides abundant active sites for heavy metal cations binding. This study provides a potential green modification method for agricultural waste valorization for heavy metal removal and environmental remediation.

Keywords: sweet sorghum straw fermentation residue (FSSR); heavy metal; irradiation grafting; carboxyl group; biosorbent

1. Introduction

Heavy metal pollution, mainly caused by industrial activities such as mining, smelting, electroplating, and chemical manufacturing, has become a severe environmental problem worldwide, posing serious threats to ecological systems and human health [1]. Among various heavy metals, Cu(II), Zn(II), Pb(II), and Cr(VI) are widely present in industrial wastewater and soil; Cu(II) and Zn(II) are essential trace elements for organisms but can cause metabolic disorders and organ damage at excessive concentrations, while Pb(II) is highly toxic and can

accumulate in the human body to impair the nervous system, especially in children, and Cr(VI) exhibits strong carcinogenic, mutagenic, and teratogenic properties even at low concentrations.

Heavy metals, characterized by high toxicity, resistance to degradation, and tendency to bioaccumulate, pose severe threats to the ecological environment and human health. Conventional heavy metal treatment technologies, such as chemical precipitation, ion exchange, and membrane separation, suffer from inherent drawbacks including high operational cost, easy generation of secondary sludge, and limited treatment efficiency for low-concentration heavy metal pollution [2–4]. Biosorption has become a research hotspot in the green remediation of heavy metal pollution owing to its advantages including abundant raw materials, mild reaction conditions, and environmental friendliness. Biosorbents mainly include microorganisms, agricultural and forestry wastes, biomass-based materials, and living plants, each with distinctive application merits [5,6]. The adsorption mechanisms primarily involve ion exchange, surface complexation, and electrostatic adsorption, accompanied by physical adsorption and redox processes [7,8]. Key factors affecting adsorption performance include pH, contact time, and coexisting ions. Modification techniques such as physical, chemical, and magnetic composite modification can significantly improve the properties of adsorbents. At present, this technology has been tested in the treatment of various types of wastewaters, yet it still faces challenges such as low adsorption efficiency, insufficient selectivity, poor reusability, and difficulties in large-scale engineering application. Future development should focus on high efficiency, selectivity, and resource utilization to promote biosorption as a mainstream technology for heavy metal pollution control.

Agricultural wastes materials are abundant, low-cost, renewable, and rich in surface functional groups (such as hydroxyl group, carboxyl group and amino group) that are able to interact with heavy metals via complexation, ion exchange or reduction reactions. Among various, sweet sorghum stalk—an abundant by-product of the bioenergy and sugar industries—has garnered interest due to its high lignocellulosic content and inherent adsorption potential [9–11]. However, the unmodified sweet sorghum stalk typically displays low adsorption capacity and heavy metal selectivity, primarily owing to the limited number of active binding sites on its surface.

To address this limitation, researchers have focused on surface modification of agricultural waste materials to enhance their functional group density and adsorption performance. Carboxyl groups (-COOH) are recognized as highly effective for heavy metal sequestration, as they can form stable chelate complexes with Cu(II) [12], Zn(II) [13], Pb(II) [14] and Cr(III) [15]. Radiation-induced grafting is an effective technology to introduce carboxyl groups onto the surface of the biosorbents via γ rays without chemical initiators or crosslinking agents, ensuring higher product purity. It controls energy penetration to realize surface-dominated grafting, significantly reducing homopolymerization, gelation and pore blockage; it operates under normal temperature and pressure, causing less damage to biomass skeletons (e.g., cellulose, chitosan) and better retaining mechanical stability; additionally, grafting yield can be precisely controlled by adjusting irradiation parameters, facilitating the regulation of surface active sites. Hakimi et al. synthesized cellulose nanofiber-grafted poly(methacrylic acid) at varying radiation doses and ligand concentrations to maximize carboxyl density [16]. However, the modified biomass material is not used for the adsorption of heavy metal. Wang et al. prepared a carboxyl-functionalized adsorbent by grafting acrylic acid onto a covalent organic framework via gamma-ray radiation, achieving efficient adsorption of Cu(II) and Pb(II) [17]. Lin et al. prepared hierarchically porous nitrogen-doped carbon for Cr(VI) removal [18]. However, the adsorbent substrates were not biomass-based materials. Our previous work reported that carboxyl-functionalized sweet sorghum stalk exhibited enhanced Cu(II) adsorption compared to the unmodified material [8]. There are few reports on the graft modification of biomass substrates for synthesizing new adsorbents used in heavy metal adsorption.

This study aimed to optimize the synthesis of carboxyl-functionalized sweet sorghum stalk fermentation residue grafted by acrylamide, ethylenediamine and then succinic anhydride (FSSR-g-AAm-EDA-SA, abbreviated as FSSR-AES) and to apply the novel modified biosorbent for adsorption of Cu(II), Zn(II), Pb(II) cations and Cr(VI) anions from aqueous solution. Specifically, FSSR was used as the backbone for graft copolymerization with acrylamide via Co-60 γ-ray irradiation—a green and efficient method that eliminates the need for chemical initiators. Subsequently, the grafted product was reacted with ethylenediamine and succinic anhydride to further introduce and enhance carboxyl group density on the material surface.

The objective of this study was to optimize the conditions for acrylamide grafting onto FSSR via Co-60 irradiation, including irradiation dose and monomer concentration; to characterize the chemical structure and surface properties of the carboxyl-functionalized FSSR-AES; to evaluate the adsorption performance of FSSR-AES for Cu(II), Zn(II), Pb(II) cations and Cr(VI) anions under different temperature conditions, and to determine the adsorption capacity; to investigate the adsorption mechanism by fitting experimental data to various isothermal models; and to compare the adsorption performance of FSSR-AES with other reported biosorbents to validate its competitiveness.

2. Materials and Methods

2.1. Carboxyl-Functionalization of FSSR

Five grams of FSSR were added to 50 mL of N, N-Dimethylacetamide (DMAC) and immersed for swelling at 100 °C for 3 h. The swollen FSSR was filtered after cooling, and a predetermined amount of acrylamide and 0.5% (*w*/*v*) of the polymerization inhibitor ferrous ammonium sulfate were added to form a 50 mL reaction system. Nitrogen gas was purged into the system for 15 min to remove dissolved oxygen, followed by overnight standing. The graft copolymerization reaction was initiated by irradiation with a Co-60 source at a specified dose. The irradiated product was washed with 100 °C hot water for 6 h to remove homopolymers, filtered, and dried at 70 °C for subsequent use. 10 g of the purified grafted product were refluxed in 100 mL of ethylenediamine for 8 h. The resulting product was separated, washed and dried. Next, 10 g of the dried product were transferred to 100 mL of a 1,4-dioxane solution containing 10 g of succinic anhydride (adjusted to pH 4.0) and refluxed for 6 h to introduce carboxyl groups. The carboxylated product was separated, washed, and dried at 60 °C to obtain FSSR-AES. The yields were 80.3 ± 2.3%. The purities were 94.6 ± 1.2%.

Figure 1 illustrates the chemical mechanism for the carboxylation modification of FSSR. Sweet sorghum stalk (SSR) was treated via ethanol fermentation to produce FSSR, which possessed a significantly higher content of hydroxyl groups (denoted as FSSR-OH) than the pristine SSR. Under γ-ray irradiation, acrylamide monomers were grafted onto the hydroxyl active sites of FSSR. Subsequently, ethylenediamine was reacted with the amino sites of the grafted acrylamide under reflux at 100 °C in toluene. Finally, grafting with acid anhydride was conducted under reflux at 90 °C in 1,4-dioxane, thereby achieving the carboxylation modification of FSSR.

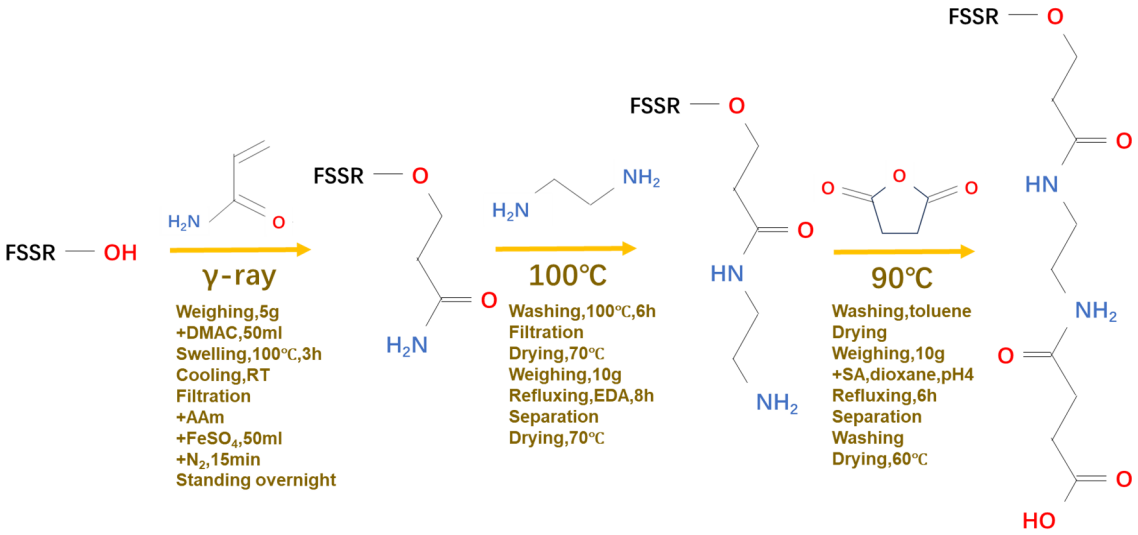

Figure 1. Schematic diagram of carboxyl-functionalization of FSSR.

2.2. Optimization of Modification Conditions

2.2.1. Irradiation Dose

After DMAC pretreatment, 5 g of FSSR was mixed with 5 g of acrylamide and 0.5% (*w*/*v*) of the polymerization inhibitor ferrous ammonium sulfate to form a 50 mL reaction system. The system was purged with nitrogen for 15 min and irradiated with a Co-60 source at doses of 2.5, 5.0, 7.5, 10.0, and 15.0 kGy, respectively. The grafting rate was computed to pinpoint the optimal irradiation dose. One-way analysis of variance (ANOVA) was used to verify the significance of the experimental results, and the statistical analysis was performed using Origin 2021 software (OriginLab Corporation, Northampton, MA, USA).

2.2.2. Monomer Concentration

After DMAC pretreatment, 5 g of FSSR were mixed with varying amounts of acrylamide (1.0, 2.5, 5.0, 7.5, and 10 g, corresponding to monomer concentration of 2%, 5%, 10%, 15%, and 20% (*w*/*v*) in the 50mL system) and 0.5% (*w*/*v*) ferrous ammonium sulfate. The system was purged with nitrogen for 15 min and irradiated at 10 kGy. The effect of monomer concentration on grafting yield was then evaluated. One-way ANOVA was used to verify the significance of the experimental results, and the statistical analysis was performed using Origin 2021 software.

2.3. Adsorption Experiment

2.3.1. Static Adsorption Experiment

A predetermined amount of FSSR-AES was added to 15mL of heavy metal stock solution with the initial concentrations of the metal ion solutions were 25, 50, 75, 100, 150, 200, and 250 mg/L, prepared from $CuCl_2$, $ZnCl_2$, $PbCl_2$, and $K_2Cr_2O_7$, respectively. For the adsorption of Cu(II), Zn(II), and Pb(II) cations, the initial pH was adjusted to 6.0, and the equilibrium time was 4 h. For Cr(VI) anions, the initial pH was set to 2.0 with an equilibrium time of 24 h. The adsorbent dosage was 0.1 g for Cu(II), Zn(II), and Cr(VI) adsorption, while 0.05 g of adsorbent was used for Pb(II) adsorption. A constant-temperature shaker, running at 150 rpm, was used to process the mixture. For each experimental condition, one blank sample and three parallel samples were prepared to ensure data reliability. The concentrations of Cu(II), Zn(II) and Pb(II) cations and total chromium were measured using an atomic absorption spectrophotometer (AAS, Jena Vario 6, Analytik Jena AG, Jena, Germany), while the Cr(VI) concentration was measured via the diphenylcarbazide spectrophotometric method. Static adsorption experiments were performed to assess the adsorption performance of FSSR and FSSR-AES for the target heavy metal ions.

2.3.2. Adsorption Isotherm Experiment

The adsorption isotherms were investigated at different temperatures (283.15 K, 293.15 K, 303.15 K, and 313.15 K). All experimental data were collated and plotted using Origin 2021 software. Fitting of the adsorption isotherm data was conducted using the Langmuir, Freundlich, Temkin and Redlich-Peterson (R-P) [19]. The fitting accuracy was evaluated based on the correlation coefficient (R^2) values.

2.4. Characterization of Adsorbents

Scanning electron microscope (SEM) was analysis was performed using Fei Quanta 200FEG field scanning electronic microscope (FEI, now Thermo Fisher Scientific, Eindhoven, The Netherlands). Fourier-transform infrared spectroscopy (FTIR) was conducted using Perkin Elmer GX spectrometer (PerkinElmer, Inc., Waltham, MA, USA) to analyze the chemical functional groups. The carboxyl group concentration of the materials was determined via acid-base titration.

2.5. Analysis of Interaction between Cr and Adsorbents

FSSR-AES samples after Cr(VI) adsorption were ground into a fine powder, sieved through a 400-mesh sieve, and fixed on adhesive tape for X-ray absorption near-edge structure (XANES) spectroscopy. $K_2Cr_2O_7$ and CrO_3, Cr_2O_3 and $Cr(NO_3)_3$ were selected as reference materials for Cr(VI) and Cr(III). XANES experiments were carried out at the synchrotron radiation facility (Institute of High Energy Physics, Chinese Academy of Sciences, Beijing). Reference samples were measured in transmission mode, while Cr-adsorbed FSSR-AES (FSSR-AES-Cr) samples were measured in fluorescence mode. IFEFFIT software (Interactive XAFS Analysis, Matt Newville, CARS, University of Chicago, USA, open-source software) was utilized for the processing and analysis of the spectra.

After DMAC pretreatment, 5 g of FSSR was mixed with 5 g of acrylamide and 0.5% (*w*/*v*) of the polymerization inhibitor ferrous ammonium sulfate to form a 50 mL reaction system. The system was purged with nitrogen for 15 min and irradiated with a Co-60 source at doses of 2.5, 5.0, 7.5, 10.0, and 15.0 kGy, respectively. The grafting rate was computed to pinpoint the optimal irradiation dose.

3. Results and Discussion

3.1. Grafting Condition Optimization

3.1.1. Effect of Irradiation Dose

The influence of dose (2.5–15.0 kGy) on acrylamide grafting rate onto FSSR is illustrated in Figure 2a. One-way ANOVA analysis showed that there were significant differences among groups ($F = 9.800$, $p = 0.014 < 0.05$). There were significant differences in the grafting rate under different irradiation doses ($p < 0.05$), indicating that the irradiation dose had a significant effect on the grafting reaction. The grafting rate increased linearly when dose increased. When the irradiation dose was further increased to 15.0 kGy, the rate of in grafting yield slowed significantly. This phenomenon can be explained by two competing effects: on one hand, increasing the irradiation dose promotes the generation of free radicals on FSSR backbone, thereby facilitating graft copolymerization and improving the grafting rate. On the other hand, excessive irradiation dose increases the probability of

homopolymerization between acrylamide monomers, leading to the formation of gel-like flocs in the reaction system. These flocs increase the viscosity of the medium, which retards the diffusion of monomers to the FSSR surface [20]. Additionally, high irradiation doses may induce radiation degradation of the FSSR matrix [21], further limiting the improvement of grafting rate. These results indicated that the optimal radiation dose was 10.0 kGy, corresponding to a maximum grafting rate of 14.6%.

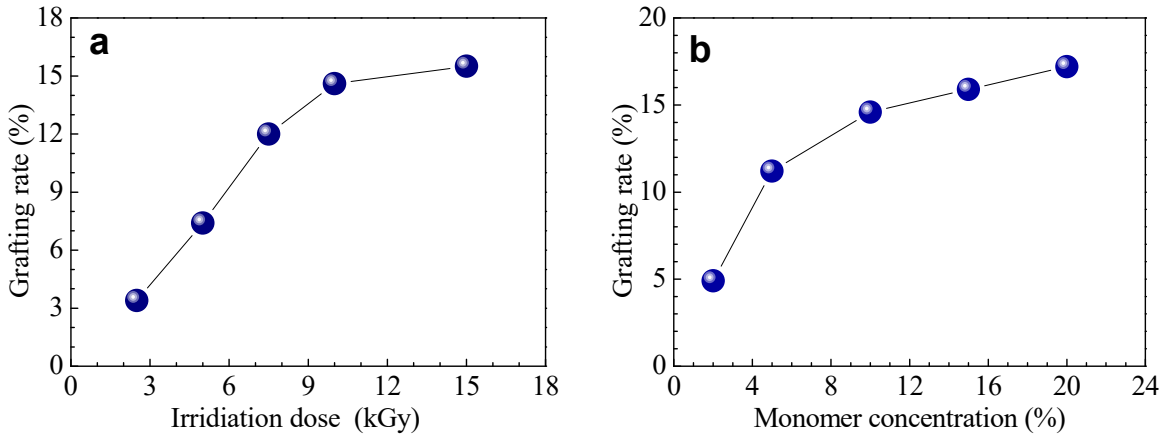

Figure 2. Effect of (**a**) irradiation dose and (**b**) monomer concentration on acrylamide grafting.

3.1.2. Effect of Acrylamide Monomer Concentration

Figure 2b shows the relationship between acrylamide monomer concentration and grafting yield under the condition of a 10.0 kGy radiation dose. The grafting rate increased rapidly from 5 to 11% as the monomer concentration increased from 2 to 5%. With further increases in monomer concentration, the rate of increase in grafting yield slowed down substantially. When the monomer concentration was increased to 20% (four times the 5% concentration), the grafting rate only reached 17.1%, which is merely 1.5 times higher than that at 5% concentration. One-way ANOVA analysis showed that there were significant differences among groups ($F = 9.325$, $p = 0.015 < 0.05$). There were significant differences in the grafting rate under different monomer concentrations ($p < 0.05$), indicating that the acrylamide concentration had a significant effect on the grafting reaction.

The initial increase in grafting rate with monomer concentration can be attributed to the enhanced contact probability between acrylamide monomers and the active sites on the FSSR backbone. However, once all active sites on the FSSR surface are saturated, additional monomers cannot participate in the graft copolymerization reaction, resulting in a plateau in the grafting rate. Moreover, high monomer concentrations increase the viscosity of the reaction system, reducing the mass transfer efficiency of monomers to the FSSR surface and promoting homopolymerization. From both economic and efficiency perspectives, the optimal monomer concentration was identified as 5%.

The relatively low grafting yield of 17.1 at maximum in this study may be attributed to the competitive homopolymerization of monomers in the solution during irradiation grafting, which reduced the efficiency of grafting onto the substrate surface. It may also result from diffusion constraints that prevented monomers from fully penetrating into the internal pores of the material, leading to uneven grafting mainly on the outer surface. To avoid excessive degradation of the biomass skeleton and maintain its structural integrity, the reaction conditions including irradiation dose, monomer concentration and reaction time were not further optimized in the present study.

3.2. Isothermal Adsorption Performance of FSSR-AES

3.2.1. Adsorption of Typical Heavy Metal Cations

The isothermal adsorption curves of FSSR-AES for Cu(II), Zn(II) and Pb(II) are presented in Figure 3a–c, respectively. At temperatures of 283.15, 293.15, 303.15 and 313.15 K, the equilibrium adsorption capacities (q_e) of FSSR-AES for Cu(II) were 19.15, 19.37, 20.84, and 21.57 mg/g, respectively, showing a slight increase with rising temperature. For Zn(II), the q_e values were 18.42, 21.48, 23.32, and 25.41 mg/g at the corresponding temperatures, representing an approximate 40% increase as the temperature increased from 283.15 to 313.15 K. For Pb(II), the q_e values were 35.67, 36.12, 40.74, and 41.85 mg/g, with an approximate 20% increase over the temperature range. These results indicate that the order of temperature sensitivity for adsorption capacity is Zn(II) > Pb(II) > Cu(II), suggesting that higher temperatures are generally favorable for the adsorption.

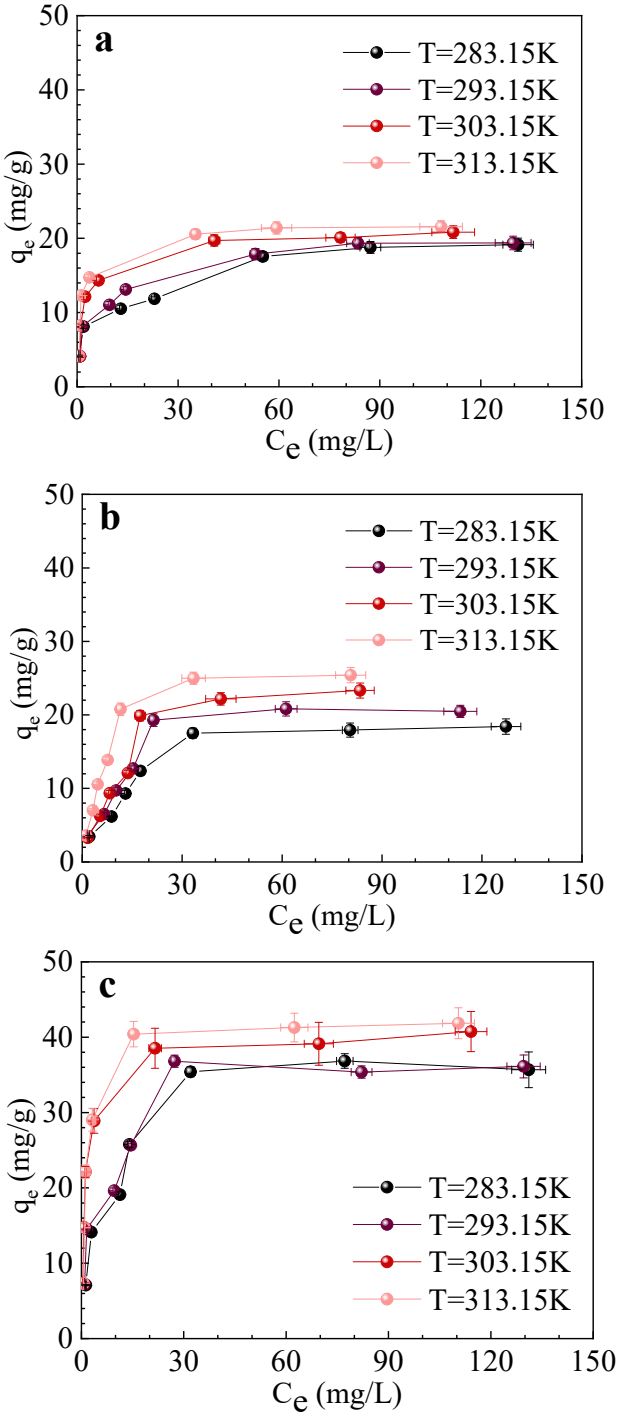

Figure 3. Isothermal adsorption curves of FSSR-AES for (a) Cu(II), (b) Zn(II) and (c) Pb(II) at different temperatures.

3.2.2. Isothermal Model Fitting for Heavy Metal Cations

Cu(II) Adsorption. The fitting results of various isothermal models for Cu(II) adsorption onto FSSR-AES are summarized in Table 1. That Cu(II) adsorption at low temperatures is better described by the Freundlich model (R^2 of 0.980 at 283.15 K and 0.972 at 293.15 K). It approximates Langmuir model under high-temperature conditions (R^2 of 0.979 at 303.15 K and 0.974 at 313.15 K).

The adsorption behavior of Cu(II) on carboxylated FSSR differs significantly from that on unmodified FSSR. For unmodified FSSR, Cu(II) adsorption was well fitted by the Freundlich model rather than the Langmuir model across all four temperatures [10], indicating that the adsorption process is dominated by weak interactions and corresponds to heterogeneous multilayer physisorption. In contrast, carboxylation modification grafts carboxyl groups onto the FSSR surface, enabling the transformation to homogeneous monolayer chemisorption dominated by strong chemical bonds at relatively high temperatures.

Table 1. Fitted parameters of isothermal models for Cu(II) adsorption onto FSSR-AES.

Model	Temperature (K)			
	283.15	**293.15**	**303.15**	**313.15**
Langmuir				
q_m (mg/g)	18.4 ± 1.3	19.2 ± 1.2	20.7 ± 1.1	21.7 ± 1.1
K_L (L/mg)	0.191 ± 0.077	0.233 ± 0.078	0.476 ± 0.116	0.699 ± 0.015
R^2	0.892	0.948	0.979	0.974
Freundlich				
K_F (mg/g)	5.81 ± 1.07	6.46 ± 1.03	8.48 ± 0.98	9.57 ± 0.95
n	3.93 ± 0.70	4.15 ± 0.69	4.92 ± 0.74	5.21 ± 0.73
R^2	0.980	0.972	0.931	0.916

Zn(II) Adsorption. The fitting results of isothermal models for Zn(II) adsorption are presented in Table 2. Both the Langmuir model and R-P model exhibited excellent fitting performance, with R^2 values greater than 0.946 across all four temperatures. In contrast, the Freundlich and Temkin models showed poor fitting, with R^2 values below 0.9, and the exponent values (β_{RP}) were all 1.00 at the four tested temperatures. The Zn(II) adsorption process onto FSSR-AES follows homogeneous monolayer chemisorption.

Zn(II) adsorption on FSSR-AES is also distinct from that on unmodified FSSR. For unmodified FSSR, the adsorption was well described using the Freundlich model rather than the Langmuir model across all four temperatures, suggesting that the adsorption process is dominated by weak interactions and corresponds to heterogeneous multilayer physisorption. On the contrary, carboxylation modification grafts carboxyl functional groups onto the FSSR surface, which provides abundant specific binding sites for Zn(II) ions and thus transforms the adsorption mechanism into monolayer chemisorption driven by strong chemical interactions.

Table 2. Fitted parameters of isothermal models for Zn(II) adsorption onto FSSR-AES.

Model	Temperature (K)			
	283.15	**293.15**	**303.15**	**313.15**
Langmuir				
q_m (mg/g)	21.6 ± 2.0	24.4 ± 2.1	28.9 ± 2.6	29.5 ± 2.0
K_L (L/mg)	0.068 ± 0.020	0.080 ± 0.021	0.068 ± 0.017	0.131 ± 0.027
R^2	0.964	0.946	0.951	0.974
Freundlich				
K_F (mg/g)	4.27 ± 1.49	5.12 ± 1.47	4.59 ± 1.32	6.94 ± 1.40
n	3.09 ± 0.83	3.13 ± 0.74	2.55 ± 0.51	3.09 ± 0.56
R^2	0.899	0.874	0.890	0.884
Temkin				
A (L/g)	0.91 ± 0.53	1.17 ± 0.59	0.80 ± 0.29	1.54 ± 0.57
B (J/mol)	245 ± 45	231 ± 37	186 ± 26	194 ± 24
R^2	0.904	0.873	0.900	0.925

Pb(II) Adsorption. Redlich-Peterson (R-P) ($R^2 > 0.944$) and Langmuir ($R^2 > 0.936$) models achieved the best fitting effects across all tested temperatures (Table 3). In contrast, the Freundlich and Temkin models showed unsatisfactory fitting performance, with R^2 values below 0.9. The exponent values (β_{RP}) of the R-P model ranged from 0.91 to 1.00, indicating that the R-P model is highly consistent with Langmuir model. Thus, the adsorption of Pb(II) onto FSSR-AES is dominated by homogeneous monolayer chemisorption.

For the unmodified FSSR, Pb(II) adsorption was well described by the Freundlich model rather than the Langmuir model at all four temperatures, suggesting that the adsorption process was dominated by heterogeneous multilayer physisorption before modification. After carboxylation modification, carboxyl functional groups were grafted onto the FSSR surface, and the adsorption of Pb(II) was transformed into homogeneous monolayer chemisorption driven by strong chemical bonds.

Max adsorption capacities of FSSR-AES for Cu(II), Zn(II) and Pb(II), derived from the Langmuir model fitting, were determined to be 21.7 ± 1.1, 29.5 ± 2.0 and 43.1 ± 1.8 mg/g, respectively. Relative to Cu(II) and Zn(II), the enhanced adsorption capacity of Pb(II) is attributable to the combined effects of its higher electronegativity and smaller ionic radius, which enable more robust interactions with the carboxyl moieties on FSSR-AES.

Table 3. Fitted parameters of isothermal models for Pb(II) adsorption onto FSSR-AES.

Model	Temperature (K)			
	283.15	**293.15**	**303.15**	**313.15**
Langmuir				
q_m (mg/g)	39.2 ± 2.4	37.3 ± 2.1	40.6 ± 1.7	43.1 ± 1.8
K_L (L/mg)	0.139 ± 0.035	0.216 ± 0.059	0.764 ± 0.146	0.634 ± 0.111
R^2	0.966	0.936	0.990	0.980
Freundlich				
K_F (mg/g)	11.4 ± 2.7	12.9 ± 2.8	18.5 ± 2.6	19.0 ± 2.5
n	3.85 ± 0.91	4.32 ± 1.04	5.45 ± 1.12	5.27 ± 1.03
R^2	0.912	0.903	0.902	0.870
Temkin				
A (L/g)	2.5 ± 1.6	5.1 ± 3.7	23.4 ± 17.9	17.1 ± 11.7
B (J/mol)	150 ± 24	177 ± 28	197 ± 28	184 ± 25
R^2	0.925	0.900	0.913	0.874
Redlich-Peterson				
K_{RP} (L/g)	5.6 ± 2.4	13.2 ± 6.5	31.1 ± 8.9	26.4 ± 6.6
α_{RP} (L/mg)$^{\beta}$	0.151 ± 0.137	0.530 ± 0.405	0.771 ± 0.378	0.587 ± 0.269
β_{RP}	0.99 ± 0.11	0.91 ± 0.07	1.00 ± 0.06	1.00 ± 0.06
R^2	0.966	0.944	0.990	0.975

3.2.3. Adsorption of Typical Heavy Metal Anions (Cr(VI))

The isothermal adsorption curves of FSSR-AES for Cr(VI) and total Cr are presented in Figure 4a,b. At temperatures of 283.15, 293.15, 303.15 and 313.15 K, the equilibrium adsorption capacities (q_e) of FSSR-AES for Cr(VI) are 28.01, 29.96, 32.96, and 33.86 mg/g, respectively. With the increase of temperature, the q_e values increased by approximately 20%. For total Cr, the q_e values at the corresponding temperatures were 10.01, 12.18, 14.18, and 15.17 mg/g, respectively.

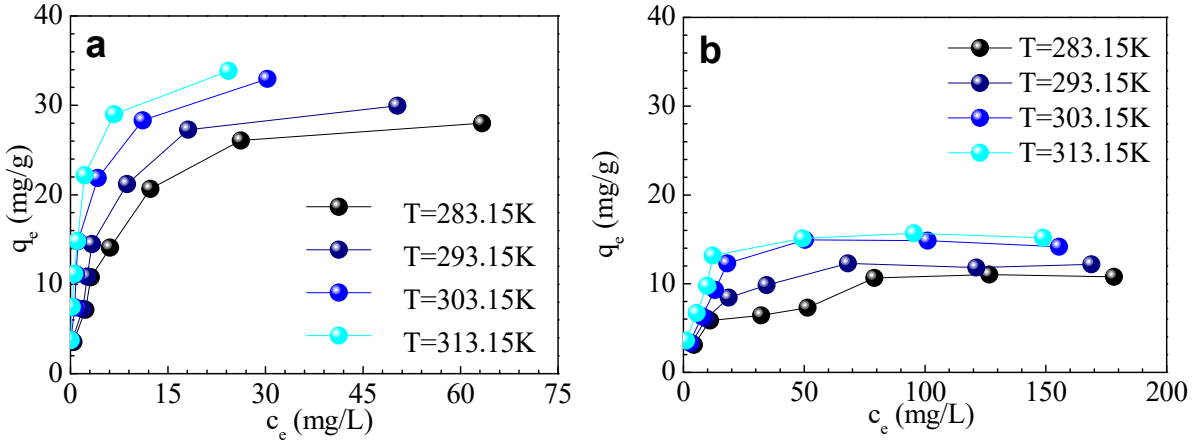

Figure 4. Isothermal adsorption curves of FSSR-AES for (**a**) Cr(VI) and (**b**) total Cr at different temperatures.

This phenomenon can be explained by the dual mechanism of Cr(VI) removal by FSSR-AES: reduction and adsorption. In Figure 4, the sorption amount of Cr(VI) is much higher than that of total Cr. During the adsorption process, Cr(VI) is first reduced to Cr(III) by the adsorbent, and then the Cr(III) cations are further adsorbed by the adsorbent, thereby being removed from the aqueous solution. The adsorption capacities of Cr(VI) and total Cr were measured and calculated based on the initial and residual concentrations in the aqueous solution. Before the adsorption experiment, only Cr(VI) existed in the aqueous solution and no Cr(III) was present. After adsorption, residual Cr(VI) and reduced Cr(III) remained in the aqueous solution. The adsorbed amount of Cr(VI) includes both the Cr(VI) directly adsorbed by the adsorbent and the Cr(VI) reduced to Cr(III). The adsorbed amount of total Cr includes both the Cr(VI) directly adsorbed by the adsorbent and the Cr(III) adsorbed by the adsorbent. The reason why the adsorption capacity of Cr(VI) is much higher than that of total Cr is that the amount of Cr(VI) reduced to Cr(III) is higher than the amount of Cr(III) subsequently adsorbed. The Cr(VI) reduced to Cr(III) is counted in the adsorbed amount of Cr(VI) but not in the adsorbed amount of total Cr. The low pH leads to protonation of FSSR-AES surface, which hinders Cr(III) diffusion to the material surface. As a consequence, part

of the Cr(III) ions produced by reduction are released into the solution, which accounts for the lower adsorption capacity of the adsorbent for total Cr relative to that for Cr(VI) [11].

3.2.4. Isothermal Model Fitting for Heavy Metal Anions

Cr(VI) Adsorption. The fitting results of isothermal models for Cr(VI) adsorption are summarized in Table 4. R-P and Langmuir models exhibited best fitting performance, with the R^2 values greater than 0.985 for R-P and 0.981 for Langmuir. In contrast, the Freundlich and Temkin models yielded relatively low R^2 values. The exponent values (β_{RP}) of the R-P model ranged from 0.914 to 1.000, suggesting that the R-P model approximates the Langmuir model. Adsorption of Cr(VI) onto FSSR-AES follows homogeneous monolayer chemisorption, even under low-temperature conditions. The adsorption mechanism of Cr(VI) is mainly governed by the reduction reaction followed by the reduced Cr(III) adsorption.

For unmodified FSSR, Cr(VI) adsorption was well described only by the Freundlich model instead of the Langmuir model across all four temperatures, suggesting that the adsorption process was dominated by heterogeneous multilayer adsorption before modification. After carboxylation modification, the abundant carboxyl groups were grafted onto FSSR-AES, and Cr(VI) adsorption was transformed into homogeneous monolayer chemisorption driven by the reduction reaction of Cr(VI).

Table 4. Fitted parameters of isothermal models for Cr(VI) adsorption onto FSSR-AES.

Model	Temperature (K)			
	283.15	**293.15**	**303.15**	**313.15**
Langmuir				
q_m (mg/g)	31.7 ± 1.7	33.8 ± 1.7	33.9 ± 1.4	34.9 ± 1.4
K_L (L/mg)	0.148 ± 0.024	0.195 ± 0.029	0.531 ± 0.075	0.800 ± 0.112
R^2	0.992	0.987	0.981	0.984
Freundlich				
K_F (mg/g)	7.4 ± 1.2	8.8 ± 1.2	12.5 ± 1.3	15.0 ± 1.2
n	2.92 ± 0.43	2.97 ± 0.40	3.30 ± 0.42	3.58 ± 0.43
R^2	0.946	0.936	0.962	0.957
Temkin				
A (L/g)	2.6 ± 1.1	4.1 ± 16.8	17.4 ± 7.8	33.0 ± 14.9
B (J/mol)	183 ± 24	187 ± 23	218 ± 25	230 ± 25
R^2	0.952	0.923	0.924	0.940
Redlich-Peterson				
K_{RP} (L/g)	4.6 ± 1.2	6.5 ± 1.5	23.2 ± 6.5	38.0 ± 10.6
α_{RP} (L/mg)$^{\beta}$	0.14 ± 0.10	0.18 ± 0.11	0.92 ± 0.45	1.40 ± 0.62
β_{RP}	1.00 ± 0.11	1.00 ± 0.10	0.91 ± 0.07	0.91 ± 0.06
R^2	0.992	0.985	0.985	0.987

Total Cr Adsorption. The fitting results of isothermal models for total Cr adsorption are presented in Table 5. The R-P and Langmuir models showed the best fitting performance ($R^2 > 0.956$ for P-R, $R^2 > 0.934$ for Langmuir). The Freundlich and Temkin models gave relatively low R^2 values. The exponent values (β_{RP}) of the R-P model were 1.00 at the temperature of 293.15–313.15 K, indicating that the R-P model approximates the Langmuir model under high-temperature conditions. These results confirm that the adsorption of total Cr onto FSSR-AES follows homogeneous monolayer chemisorption. The adsorption mechanism of total Cr includes two steps: (1) transformation of Cr(VI) to Cr(III) via carboxyl and other functional moieties in FSSR-AES; and (2) chemisorption of Cr(III) ions onto FSSR-AES.

For unmodified FSSR, the adsorption of total Cr was best fitted by the Freundlich model, followed by the Langmuir model, while the R-P model showed poor fitting performance. After modification, the adsorption of total Cr on FSSR was well described by the R-P and Langmuir models. Carboxylation modification grafted carboxyl groups onto the adsorbent surface, which transformed the total Cr adsorption from heterogeneous multilayer adsorption to homogeneous monolayer chemisorption.

The maximum adsorption capacities of FSSR-AES for Cr(VI) and total Cr, derived from the Langmuir model fitting at 313.15 K, were determined to be 34.9 ± 1.4 and 16.5 ± 0.7 mg/g, respectively.

Table 5. Fitted parameters of isothermal models for total Cr adsorption onto FSSR-AES.

Model	Temperature (K)			
	283.15	**293.15**	**303.15**	**313.15**
Langmuir				
q_m (mg/g)	11.6 ± 0.9	13.2 ± 0.8	16.3 ± 0.8	16.5 ± 0.7
K_L (L/mg)	0.062 ± 0.020	0.094 ± 0.024	0.110 ± 0.021	0.179 ± 0.034
R^2	0.934	0.993	0.972	0.969
Freundlich				
K_F (mg/g)	2.44 ± 0.93	3.66 ± 0.98	4.73 ± 0.94	5.78 ± 0.94
n	3.31 ± 0.94	3.97 ± 0.99	4.07 ± 0.80	4.62 ± 0.87
R^2	0.952	0.939	0.878	0.898
Temkin				
A (L/g)	0.95 ± 0.72	1.51 ± 1.05	1.67 ± 0.88	4.46 ± 2.66
B (J/mol)	470 ± 94	446 ± 77	374 ± 51	436 ± 56
R^2	0.910	0.948	0.873	0.890

3.2.5. Thermodynamic Studies on Metal Ion Adsorption

The thermodynamic parameters of the adsorption process for different heavy metals were calculated and compared, and the results are summarized as Table 6. All adsorption processes were endothermic, as indicated by the positive values of enthalpy change (ΔH), which means that increasing temperature was beneficial to the adsorption reaction. Specifically, the ΔH value of Cr(VI) (high adsorption group) was the highest (44.79 kJ·mol^{-1}), followed by Pb(II) (42.33 kJ·mol^{-1}) and Cu(II) (34.31 kJ·mol^{-1}), indicating that Cr(VI) adsorption was more sensitive to temperature changes.

Table 6. Comparison table of thermodynamic parameters for heavy metal adsorption.

Heavy Metal	ΔH(kJ·mol^{-1})	ΔS (kJ·mol^{-1}·K^{-1})	ΔG (kJ·mol^{-1})			
			283.15 K	**293.15 K**	**303.15 K**	**313.15 K**
Cu(II)	34.31	0.198	−22.08	−23.41	−26.00	−27.83
Zn(II)	13.21	0.116	−19.78	−20.88	−21.16	−23.55
Pb(II)	42.33	0.235	−24.17	−26.09	−30.13	−30.66
Cr(VI)	44.79	0.232	−21.07	−22.49	−25.79	−27.69
Total Cr	24.86	0.155	−18.99	−20.72	−21.81	−23.79

In terms of entropy change (ΔS), all systems showed positive values, which indicated that the solid-liquid interface disorder degree increased during the adsorption process. Among them, the ΔS value of Pb(II) adsorption was the largest (0.235 kJ·mol^{-1}·K^{-1}), followed by Cr(VI) (0.232 kJ·mol^{-1}·K^{-1}) and Cu(II) (0.198 kJ·mol^{-1}·K^{-1}), suggesting that the interface structure change was most significant during Pb(II) adsorption.

For the Gibbs free energy (ΔG), all ΔG values were negative, indicating that the adsorption process was spontaneous. In addition, the adsorption affinity of different heavy metals was quite different: Pb(II) had the strongest adsorption affinity (ΔG = −24.17 kJ·mol^{-1} at 283.15 K), followed by Cu(II) and Cr(VI), which was related to the difference in ion radius and adsorption site interaction strength.

The adsorption thermodynamics of Cu(II), Zn(II), Pb(II), Cr(VI) and total Cr showed consistent rules: endothermic adsorption, increased interface disorder degree, and spontaneous adsorption at low concentration.

3.3. Characterization of FSSR-AES

3.3.1. SEM Analysis

The SEM images of the modified material are presented in Figure 5. The surface of FSSR-AAm-EDA (Figure 5a) exhibits a relatively smooth morphology, while the surface of FSSR-AES (Figure 5b) shows distinct wrinkles and rough textures. These morphological changes are attributed to the high-temperature reaction during the succinic anhydride modification step. Despite the surface changes, the basic structure of the sweet sorghum stalk residue is retained, which is beneficial for maintaining the mechanical stability of the adsorbent during the adsorption process.

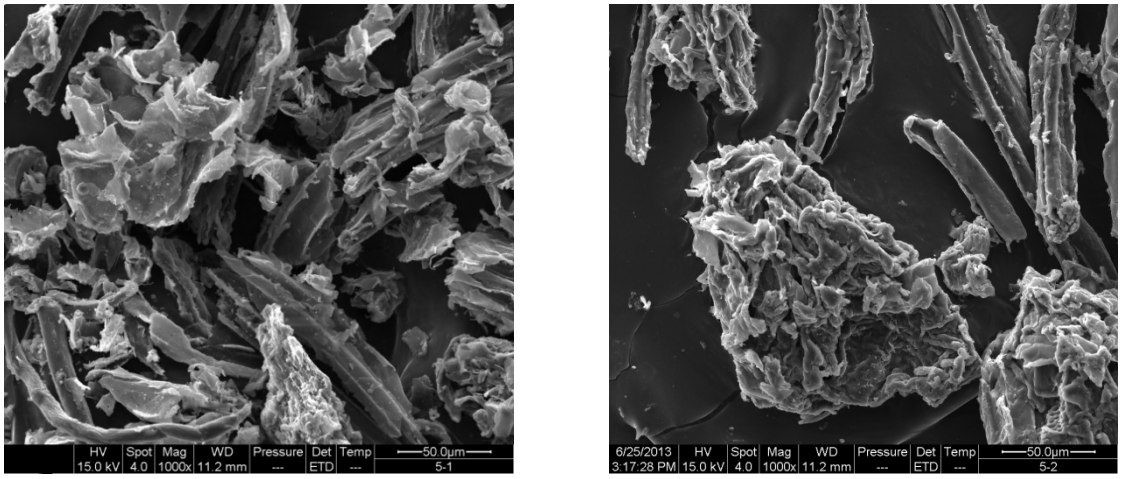

(**a**) (**b**)

Figure 5. SEM images of (**a**) FSSR-AAm-EDA and (**b**) FSSR-AES.

3.3.2. FTIR Analysis

The changes in the FTIR spectrum of the material during the carboxylation modification process are shown in Figure 6. After grafting acrylamide (AAm) onto the FSSR backbone via Co-60 γ-ray irradiation, the FTIR spectrum of grafted FSSR-AAm exhibits a clear absorption peak at 1670 cm^{-1}, corresponding to the amide group's C=O stretching vibration. Additionally, a significant enhancement is observed for the absorption peak at 3420 cm^{-1}, indicating an increase in the content of aliphatic amino groups (-NH_2). These results confirm the successful grafting of acrylamide onto the FSSR surface.

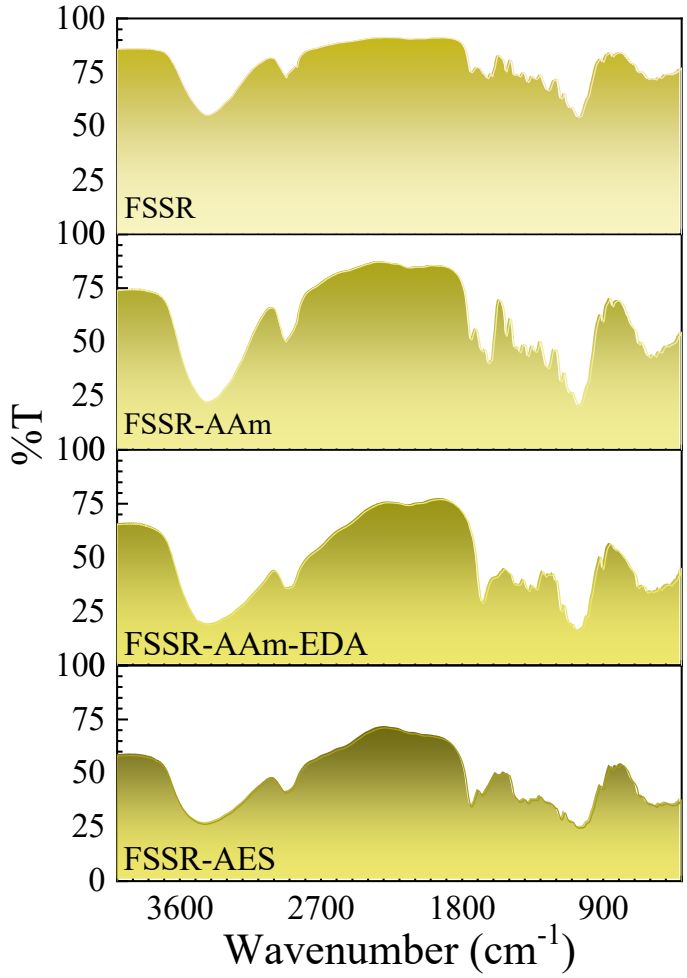

Figure 6. FTIR spectra of FSSR, FSSR-AAm, FSSR-Aam-EDA, and FSSR-AES during modification.

After the reaction of FSSR-AAm with ethylenediamine, the resulting product (FSSR-AAm-EDA) exhibits a new absorption peak at 1650 cm^{-1}, which is attributed to the stretching vibration of the amino group. Following the reaction with succinic anhydride (SA), the absorption peak at 1670 cm^{-1}(amide group) disappears, and a new absorption peak of aliphatic appears at 1737 cm^{-1}, corresponding to C=O of aliphatic carboxylic groups. These results confirm that the final product (FSSR-AES) is rich in carboxyl functional groups, which is consistent with the expected modification outcome.

3.3.3. Carboxyl Functional Group Analysis

The carboxyl group contents in FSSR-AES and FSSR were determined using the titration method. The results showed that the carboxyl content in FSSR-AES was 2.55 mmol/g, while no carboxyl functional groups were detected in FSSR before grafting. The high carboxyl group content in FSSR-AES significantly enhances its adsorption performance for heavy metal cations and anions compared to unmodified FSSR [10,11]. These results confirm that carboxyl functional groups play a crucial role in the elimination of heavy metal from aqueous solutions.

3.3.4. XANES Analysis

The normalized XANES spectra of the reference material and adsorbent samples are presented in Figure 7. Three hexavalent chromium reference materials ($K_2Cr_2O_7$, CrO_3) and two trivalent chromium reference materials (Cr_2O_3, $Cr(NO_3)_3$) were used in this study. The characteristic peak positions of Cr(VI) and Cr(III) reference materials are significantly different: the Cr(VI) reference materials exhibit a pre-edge peak at 5990–5995 eV before the main adsorption peak, while the Cr(III) reference materials show a characteristic peak at approximately 6110 eV.

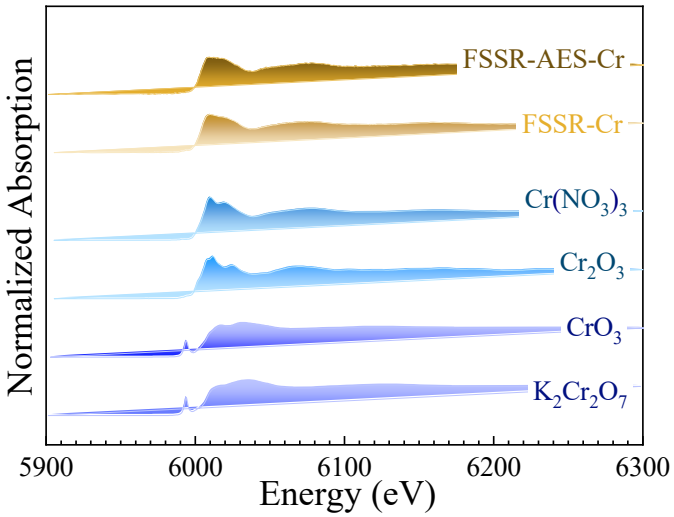

Figure 7. Normalized XANES spectra of reference materials and Cr-adsorbed adsorbent samples.

The XANES spectra of the FSSR and FSSR-AES samples after Cr(VI) absorption are consistent with the spectra of the Cr(III) reference materials, with no pre-edge peak observed at 5990 eV. These results confirm that the Cr species adsorbed onto the material surface exists in the form of Cr(III), indicating that Cr(VI) was first reduced to Cr(III), which was then adsorbed onto the carboxyl groups. There was no significant difference in peak position and peak height among the XANES spectra of the adsorbent samples.

3.4. Adsorption Performance of FSSR-AES

3.4.1. Adsorption Mechanisms

The adsorption of three heavy metal cations, namely Cu(II), Zn(II), Pb(II), and the Cr(VI) anion by FSSR-AES is a multi-mechanism coupling process based on the synergistic effect of material pretreatment and functional modification via irradiation grafting. Figure 8 shows a schematic diagram of the adsorption mechanism. Its core mechanism starts with ethanol fermentation pretreatment of sweet sorghum straw: FSSR is prepared from sweet sorghum straw after ethanol fermentation, during which partial lignin and hemicellulose are degraded, breaking the dense structure of the material, fully exposing the originally encapsulated cellulose skeleton, and significantly increasing the number of surface hydroxyl groups (-OH). This provides sufficient active sites for subsequent γ-ray irradiation grafting, thereby facilitating the smooth progress of acrylamide grafting, ethylenediamine grafting, and

acid anhydride grafting reactions, ultimately achieving efficient loading of carboxyl groups (-COOH). Meanwhile, the reducing substances and porous structure derived from fermentation are retained, laying the foundation for the adsorption of various heavy metals. Subsequent irradiation grafting further introduces synergistic carboxyl groups, constructing an adsorption system with simultaneous reduction, ion exchange, and electrostatic adsorption capabilities.

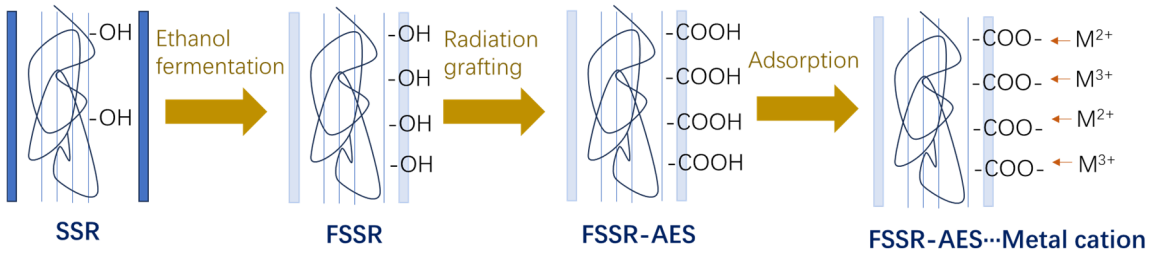

Figure 8. Schematic diagram of the adsorption mechanism.

For the three heavy metal cations Cu(II), Zn(II), and Pb(II), carboxyl groups dissociate in aqueous solution to form negatively charged -COO^-, which undergoes ion exchange with the cations (-COO^- replaces the dissociated H^+ via cation exchange). A higher carboxyl content corresponds to more active sites, stronger adsorption capacity, and higher affinity. For Cr(VI), its adsorption exhibits a two-step synergistic "reduction–adsorption" characteristic. Since Cr(VI) mainly exists as anions such as $Cr_2O_7^{2-}$ and CrO_4^{2-} in aqueous solution, the negatively charged dissociated carboxyl groups generate electrostatic repulsion against Cr(VI) anions, meaning carboxyl groups themselves are unfavorable for direct Cr(VI) adsorption. However, the reducing substances retained in FSSR after ethanol fermentation (e.g., polyphenols, reducing sugars) and the reducing sites generated by irradiation can reduce highly toxic and mobile Cr(VI) to low-toxicity and easily immobilized Cr(III) cations. At this stage, carboxyl groups play a core adsorption role, firmly adsorbing the in-situ reduced Cr(III) through ion exchange and electrostatic attraction, assisted by physical adsorption for further immobilization, thus achieving removal of Cr(VI). In other words, although carboxyl groups do not directly participate in Cr(VI) adsorption, they act as key sites to "capture" the reduced Cr(III), indirectly enhancing the overall chromium removal efficiency. The adsorption of the four heavy metals by FSSR-AES is dominated by chemisorption.

3.4.2. Adsorption Performance in the Ternary System of Cu(II), Zn(II) and Pb(II)

The isothermal adsorption curves of FSSR-AES for the ternary system of Cu(II), Zn(II) and Pb(II) are shown in Figure 9. The average adsorption capacities of Pb(II), Zn(II) and Cu(II) are 24.40, 4.40 and 2.71 mg/g, respectively, with an order of Pb(II) > Cu(II) > Zn(II) at c_e of 50–175 mg/L, 313.15 K. In the single system, the adsorption capacities of Pb(II), Cu(II) and Zn(II) are 41.67, 21.49 and 25.57 mg/g, respectively, with an order of Pb(II) > Zn(II) > Cu(II) (at c_e = 50–175 mg/L, 313.15 K). In the multi-component system, the adsorption capacity of each metal ion decreases compared with that in the single system, and the order of adsorption capacity is inconsistent with that in the single system. The adsorption capacity of FSSR-AES for Pb(II) is much higher than those for Cu(II) and Zn(II), and the adsorption capacity for Cu(II) is also higher than that for Zn(II). It can be seen that carboxyl functional groups exhibit strong selective adsorption performance toward Pb(II).

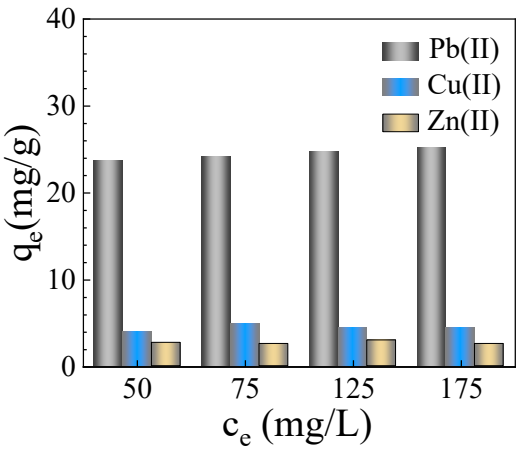

Figure 9. Isothermal adsorption curves of FSSR-AES for the ternary system of Cu(II), Zn(II) and Pb(II).

3.4.3. Comparison of Adsorption Performance with Other Biosorbents

Tables 7–10 summarized the adsorption capacities of biomass adsorbents and modified materials (mainly composed of cellulose, lignin, etc.) for Cu(II), Zn(II), Pb(II) and Cr(VI), as well as the fitting results of isothermal adsorption models. The adsorption capacities of unmodified natural materials (e.g., flax, fruit shells, leaves) are relatively low, and different natural materials exhibit distinct adsorption performances for heavy metal ions due to their varying physical and chemical properties. In contrast, the adsorption capacity of biomass materials is significantly enhanced after modification. Modification methods mainly focus on introducing or improving surface functional groups to enhance the ion-exchange capacity of the adsorbents.

Mzinyane modified pinecone powder with acrylic acid for Cu(II) and Zn(II) adsorption, investigating the chelation effect of poly(hydroxamic acid) ligands [22]. Mahour et al. prepared a carboxyl-modified seed composite for Pb(II) adsorption [23]. Jiang et al. grafted polyacrylamide onto bagasse cellulose to introduce amino ligands for Pb(II) adsorption [24]. Zhao et al. prepared a carboxylated loofah sponge adsorbent via irradiation for Pb(II) adsorption [25]. Popovic et al. grafted polyethyleneimine onto a lignin matrix to fabricate an aminated biosorbent for Cr(VI) adsorption [26]. Huang et al. grafted amino, pyridyl and pyrazinyl groups onto cotton fiber surfaces to enhance the reduction and adsorption of Cr(VI) [27]. Li et al. fabricated a novel adsorbent using electrolytic manganese residue (EMR) and chitosan (CS), where the electrostatic adsorption between $–NH_3^+$ and Cr(VI) anions is strengthened, and the transformer of Cr(VI) to Cr(III) by hydroxyl groups is enhanced, followed by the chelation of Cr(III) with CS [28]. Yogeshwaran and Priya utilized Sargassum Wightii-brown algae for Cr, Pb and Zn removal from the aqueous solution [29]. In recent years, researchers have also made progress in the adsorption of heavy metals using pectin, algae, and sawdust [30–32]. Since adsorption capacities were not reported in these studies, they were not included in the tables for comparison.

Table 7. Comparison of biosorbents for Cu(II) adsorption.

Biosorbent	Original Material	Adsorption Capacity (mg/g)	Isotherm Model	References
FSSR-AES	Fermented sweet sorghum residues	21.7	L	This study
FSSR	-	1.94	F	[10]
Sweet sorghum residues	-	0.83	F	[11]
Cotton fiber-citric acid	Cotton fiber	6.12		[33]
Flax processing wastes	-	8.32		[34]
Marula seed husk biomass	-	10.20	L	[35]
Magnetic chitosan nanoparticles	Chitosan	35.5	L	[36]
Xanthate-modified magnetic chitosan	Chitosan	34.5	L	[37]
Flax fibers	-	7.808		[38]
Pinecone shell	-	11.1		[39]
SHI-BTCA	Chenevotte	10.86		[40]
Acrylic acid-pine cone powder	Pine cone powder	14	L	[22]
Lignocellulosic biomass of CLP	Citrus limon peel powder	76.92	L	[41]
EAA-MCSA	Chitosan/sodium alginate	85.25	L	[42]
MSCP	Sugarcane	114.02		[24]
PEI@CNF	Cellulose nanofibril aerogel	120		[43]
Modified sugarcane bagasse	Sugarcane bagasse	268.0		[44]

"-" represents the unmodified biosorbent materials.

The isothermal adsorption processes of heavy metals onto unmodified biosorbents and materials follow either the Langmuir or Freundlich model, whereas those onto modified biosorbents for Cu(II), Zn(II), Pb(II) and Cr(VI) basically conform to the Langmuir isothermal adsorption model. This is because the surface of modified materials is usually homogeneous, and the adsorption reaction generally proceeds as monolayer adsorption, where there are no mutual interactions between the heavy metal ions adsorbed on adsorbents.

The adsorption capacity of biosorbents for Cu(II) and Zn(II) are generally lower than those for Pb(II). The adsorption capacity of adsorbents varies significantly depending on the adsorbent matrix, ligand type, modification method, and adsorption test conditions, which is closely related to the adsorption mechanism. In this study, FSSR was modified with carboxyl functional groups to prepare FSSR-AES, which exhibits excellent removal efficiency for both metal cations and anions. The adsorption performance of FSSR-AES is comparable to or even better than that of many previously reported modified biomass adsorbents, highlighting its potential as an economical and green biosorbent for heavy metal removal.

Table 8. Comparison of biosorbents for Zn(II) adsorption.

Biosorbent	Original Material	Adsorption Capacity (mg/g)	Isotherm Model	References
FSSR-AES	Fermented sweet sorghum residues	29.5	L	This study
Cotton fiber-citric acid	Cotton fiber	4.53		[33]
Flax processing wastes	-	7.12		[34]
Flax fibers	-	4.615		[37]
Lantana camara leaves	-	2.778	L	[45]
Hemp biomass	-	12.97	F	[46]
Hydrodistillation residues of Centaurea nicaeensis plant	-	13.78		[47]
Green alga Neochloris oleoabundans	-	32.43		[13]
Na-SW	Soy waste biomass	31.85		[48]
Magnetized Agaricus augustus	Mushroom	49.0		[49]
Acrylic acid-pine cone powder	Pine cone powder	95.79	L	[22]
Modified sugarcane bagasse	Sugarcane bagasse	200.0		[44]

"-" represents the unmodified biosorbent materials.

Table 9. Comparison of biosorbents for Pb(II) adsorption.

Biosorbent	Original Material	Adsorption Capacity (mg/g)	Isotherm Model	References
FSSR-AES	Fermented sweet sorghum residues	43.1	L	This study
FSSR	-	6.92		[50]
Flax processing wastes	-	13.35		[34]
Marula seed husk biomass	-	20	L	[35]
Cotton fiber-citric acid	Cotton fiber	21.62		[33]
Flax fibers	-	23.184		[38]
Pinecone shell	-	66		[39]
Green alga *Neochloris oleoabundans*	-	100.1		[13]
Watermelon rind	-	230.5		[51]
Carboxyl appended polymerized seed composite	Seed composite	49.86	L	[23]
Lignocellulosic biomass of CLP	Citrus limon peel powder	100	L	[41]
MSCP	Sugarcane	165.56		[24]
LFs-PGMA-IDAA	Loofah sponge	237.85		[25]
Saccharomyces cerevisiae	-	85.57	L	[52]
Aspergillus niger	-	36.2	F	[53]
Modified sugarcane bagasse	Sugarcane bagasse	700.0		[44]
Composts	-	357		[54]

"-" represents the unmodified biosorbent materials.

Table 10. Comparison of biosorbents for Cr(VI) adsorption.

Biosorbent	Original Material	Adsorption Capacity (mg/g)	Isotherm Model	References
FSSR-AES	Fermented sweet sorghum residues	34.9	L	This study
FSSR	-	23	F	[11]
Sugarcane bagasse	-	3.956		[44]
Filamentous forms of algae	-	16.23		[55]
Cistus libanotis L. leaf	-	32.02		[56]
A-LMS	Lignin	54.20	L	[26]
C-2-APZ	Cotton	54.92	L	[27]
C-4-APD	Cotton	89.66	L	[27]
EMR-CS	Chitosan	133.64	L	[28]

"-" represents the unmodified biosorbent materials.

3.4.4. Comprehensive Analysis and Future Prospects

The cost of FSSR-AES adsorbent is estimated from raw materials, preparation process and other expenses. Raw materials account for 40–60% of the total cost, including ethanol-fermented straw, modifiers, water, electricity and gas. Preparation process costs (pretreatment, reaction and post-treatment) account for 20–30%. Other costs involve equipment maintenance, labor, management and testing. The total cost is expected to be 1800–3000 yuan/ton at scale, much lower than commercial activated carbon (3000–6000 yuan/ton). Using food waste from ethanol fermentation and optimizing the modification process can further lower the cost.

Although the FSSR-AES adsorbent prepared in this study also contains carboxyl functional groups, it differs from conventional carboxyl-modified biosorbents reported in the literature in the following aspects: Raw material source: This study uses straw from ethanol fermentation by-products as the raw material, which realizes waste valorization with green and low-cost feedstock. Preparation route: A mild preparation process of fermentation coupled with gamma-ray irradiation grafting modification is adopted, which is distinct from traditional chemical modification using strong acids and strong alkalis. Structure and adsorption performance: FSSR-AES possesses a more abundant pore structure and more carboxyl sites, and exhibits excellent selective adsorption toward Pb(II) in a ternary heavy metal coexisting system. The comparison in such systems and the cost analysis are newly added contents of this work.

This study still has several limitations: adsorption experiments were conducted with simulated rather than real wastewater, the biosorbent's recyclability was not explored, kinetic analysis and pH effects were insufficient. To address these gaps, future research will use real wastewater to test adsorption performance, conduct systematic regeneration experiments, perform in-depth kinetic and pH effects studies to clarify adsorption mechanisms, investigate selectivity in mixed systems, and explore biosorbent modification and scale-up applications to promote its practical use.

4. Conclusions

(1) The optimal conditions for acrylamide grafting onto FSSR via Co-60 γ-ray irradiation were determined as follows: irradiation dose of 10 kGy, and acrylamide monomer concentration of 5%, corresponding to a maximum grafting rate of 14.6%.
(2) The carboxyl group content on FSSR-AES was 2.55 mmol/g. FTIR characterization confirmed the successful introduction of amide, aliphatic amino, and carboxyl groups onto FSSR during the two-step modification process.
(3) At 313.15 K, the maximum adsorption capacities of FSSR-AES for Cu(II), Zn(II), Pb(II) and Cr(VI) were determined to be 21.7, 29.5, 43.1 and 34.9 mg/g, respectively. The higher adsorption of FSSR-AES compared to unmodified FSSR is attributed to its high carboxyl group content, which provides abundant active sites for heavy metal ion binding.
(4) The Langmuir and R-P isothermal models provide the best fit for the isothermal adsorption processes of Cu(II), Zn(II), Pb(II) and Cr(VI) onto FSSR-AES, indicating that the adsorption mechanism follows homogeneous monolayer chemisorption with no mutual interactions between adsorbed molecules. XANES analysis confirmed that FSSR-AES can reduce Cr(VI) to less toxic Cr(III), followed by the adsorption of Cr(III) onto the material surface via the coordination interaction with carboxyl groups.
(5) FSSR-AES exhibits excellent adsorption performance for both heavy metal cations and anions, with adsorption capacities comparable to or even better than those of many previously reported modified biomass adsorbents. This study provides a potential green modification method for agricultural waste valorization, and the prepared FSSR-AES adsorbent can be used for heavy metal removal from wastewater.

Author Contributions

J.W.: writing, methodology, investigation, data curation, supervision; J.D.: investigation, methodology, data curation; X.G.: data curation, software. All authors have read and agreed to the published version of the manuscript.

Funding

This research was funded by the National Key Research and Development Program (2016YFC1402507).

Institutional Review Board Statement

Not applicable.

Informed Consent Statement

Not applicable.

Data Availability Statement

The raw data used in this study can be obtained from the authors upon reasonable request.

Conflicts of Interest

The authors declare no conflict of interest.

Use of AI and AI-Assisted Technologies

No AI tools were utilized for this paper.

References

1. Wang, J.; Guo, X. Adsorption Kinetics and Isotherm Models of Heavy Metals by Various Adsorbents: An Overview. *Crit. Rev. Environ. Sci. Technol.* **2023**, *53*, 1837–1865.
2. Yin, Y.; Wang, J. The Evolution of Environmental Technology: From End-of-Pipe to Systemic Solutions. *Environ. Microb. Technol.* **2026**, *1*, 1.
3. Sun, Z.; Liao, Y.; Zhang, Y.; et al. Sustainable Carbon Materials in Environmental and Energy Applications. *Sustain. Carbon Mater.* **2025**, *1*, e007. https://doi.org/10.48130/scm-0025-0002.
4. Pan, X.; Ji, H.; Zhang, N.; et al. Research Progress of Graphene-Based Nanomaterials for the Environmental Remediation. *Chin. Chem. Lett.* **2020**, *31*, 1462–1473.
5. Wang, J.; Chen, C. Biosorbents for Heavy Metals Removal and Their Future. *Biotechnol. Adv.* **2009**, *27*, 195–226.
6. Karic, N.; Maia, A.S.; Teodorovic, A.; et al. Bio-Waste Valorisation: Agricultural Wastes as Biosorbents for Removal of (In)Organic Pollutants in Wastewater Treatment. *Chem. Eng. J. Adv.* **2022**, *9*, 100239.
7. Gupta, B.; Mishra, A.; Singh, R.; et al. Fabrication of Calcite Based Biocomposites for Catalytic Removal of Heavy Metals from Electroplating Industrial Effluent. *Environ. Technol. Innovation* **2021**, *21*, 101278.
8. Asaad, A.A. Sorption of Chromium from Aqueous Solutions Using *Fucus vesiculosus* Algae Biosorbent. *BMC Chem.* **2024**, *18*, 145.
9. Dong, J.; Hu, J.; Wang, J. Radiation-Induced Grafting of Sweet Sorghum Stalk for Copper(II) Removal from Aqueous Solution. *J. Hazard. Mater.* **2013**, *262*, 845–852.
10. Wu, J.; Dong, J.; Wang, J. Adsorptive Removal of Cu(II) from Aqueous Solution by Fermented Sweet Sorghum Residues as a Novel Biosorbent. *J. Mol. Liq.* **2022**, *367*, 120362.
11. Wu, J.; Dong, J.; Guo, X. Biosorption of Chromium(VI) in Aqueous Solution by Fermented Sweet Sorghum Residues: Kinetics, Isotherm and Mechanism. *Environ. Microb. Technol.* **2026**, *1*, 6.
12. Zhang, Y.; Liu, T.; Wang, B.; et al. Activating H_2S into Polysulfide by Citric Acid-Induced Surface-Active Oxygen in Cu-OMS-2 for Enhanced Oxidation of Hg^0 at Ambient Temperature. *Environ. Sci. Technol.* **2025**, *59*, 15282–15292.
13. Gu, S.; Lan, C. Effects of Culture pH on Cell Surface Properties and Biosorption of Pb(II), Cd(II), Zn(II) of Green Alga *Neochloris oleoabundans*. *Chem. Eng. J.* **2023**, *468*, 143579.
14. Lu, X.; Wang, L.; Li, J.; et al. Microplastics Inhibit Lead Binding to Sediment Components: Influence of Surface Functional Groups and Charge Environment. *Water Res.* **2025**, *281*, 123661.
15. Mao, J.; Xue, Y.; Zhu, H.; et al. Agricultural Residue-Based Adsorbents with Anisotropic Cross-Linked Structures for Simultaneous Instantaneous Capture of Heavy Metal Ions. *Chem. Eng. J.* **2024**, *482*, 149010.
16. Hakimi, N.M.F.; Mohamad, S.F.; Al Edrus, S.S.O.; et al. Radiation-Induced Admicellar Polymerization of Methacrylate Acid for pH Responsive Cellulose Nanofibrils. *Cellulose* **2024**, *31*, 279–292.
17. Wang, Y.; Wang, Y.; Liu, C.; et al. Radiation Synthesized Carboxyl-Functionalized Covalent Organic Framework Adsorbent for Efficient Heavy Metal Decontamination. *Radiat. Phys. Chem.* **2023**, *212*, 111140.
18. Lin, D.; Yang, J.; Chen, F. Hierarchically Porous Nitrogen-Doped Carbon with High Conductivity for Rapid and Efficient Cr(VI) Reduction. *Adv. Sci.* **2026**, *13*, e18926. https://doi.org/10.1002/advs.202518926.
19. Wang, J.; Guo, X. Adsorption Isotherm Models: Classification, Physical Meaning, Application and Solving Method. *Chemosphere* **2020**, *258*, 127279.
20. Azzian, M.I.M.; Mohamad, S.F.; Salleh, W.N.W.; et al. Surface Modification of PVDF Membrane by Radiation-Induced Admicellar Polymerization of Acrylamide in the Presence of Cationic Surfactant. *Radiat. Phys. Chem.* **2024**, *214*, 111309.
21. Zhou, P.; Ru, X.; Yang, W.; et al. Study on Preparation of Cationic Flocculants by Grafting Binary Monomer on Cellulose Substrate by γ-Ray Co-Irradiation. *J. Environ. Chem. Eng.* **2022**, *10*, 107138.
22. Mzinyane, N.N. Adsorption of Heavy Metal from Acid Mine Drainage Using Poly(hydroxamic acid) Ligand. *S. Afr. J. Chem. Eng.* **2022**, *42*, 318–336.
23. Mahour, S.; Verma, S.K.; Arora, J.K.; et al. Carboxyl Appended Polymerized Seed Composite with Controlled Structural Properties for Enhanced Heavy Metal Capture. *Sep. Purif. Technol.* **2022**, *284*, 120247.
24. Jiang, W.; Xing, Y.; Mo, L.; et al. Synthesis of Polyethylenimine Modified Sugarcane Bagasse Cellulose and Its Competitive Adsorption of Pb^{2+}, Cu^{2+} and Zn^{2+} from Aqueous Solution. *Desalin. Water Treat.* **2022**, *270*, 172–184.

25. Zhao, Y.; Chen, T.; Liang, T.; et al. Radiation Synthesis of IDAA Functionalized Loofah Sponge for Enhanced Removal of Pb(II) and Cd(II): Behavior and Mechanism Investigation. *J. Mol. Liq.* **2023**, *392*, 123428.
26. Popovic, A.L.; Rusmirovic, J.D.; Velickovic, Z.; et al. Novel Amino-Functionalized Lignin Microspheres: High Performance Biosorbent with Enhanced Capacity for Heavy Metal Ion Removal. *Int. J. Biol. Macromol.* **2020**, *156*, 1160–1173.
27. Huang, Z.; Wu, P.; Yin, Y.; et al. Preparation of Cotton Fibers Modified with Aromatic Heterocyclic Compounds and Study of Cr(VI) Adsorption Performance. *Cellulose* **2021**, *28*, 11037–11049.
28. Li, J.; Ke, X.; Wei, H.; et al. Insight into a Novel Composite Biosorbent by Incorporating Chitosan into Electrolytic Manganese Residue for Cr(VI) Removal from Aqueous Solutions. *Sep. Purif. Technol.* **2024**, *332*, 125778.
29. Yogeshwaran, V.; Priya, A.K. Biosorption of Heavy Metal Ions from Aqueous Solutions Using Porous *Sargassum wightii* (SW) Brown Algae: Batch Adsorption, Kinetic and Thermodynamic Studies. *Iran. J. Chem. Chem. Eng.* **2023**, *42*, 3624–3639. https://doi.org/10.30492/ijcce.2023.1974163.5731.
30. Vargas-Solano, S.V.; Lizcano-Delgado, Y.Y.; Rodriguez-Gonzalez, F.; et al. Spatial Distribution of Heavy Metals in the Water of Tequesquitengo Lake, Morelos, Mexico, and Their Biosorption by Pectin. *Water* **2025**, *17*, 2050.
31. Khan, S.; Jiang, Y.; Shen, S.; et al. Heavy Metal Uptake by *Spirogyra splendida* and *Spirogyra circumlineata*: A Sustainable Approach to Industrial Wastewater Remediation. *Water Air Soil Pollut.* **2025**, *236*, 215.
32. Kramski, D.J.; Warchol, J.; Michalak, I. Sawdust-Assisted Phytoremediation: Boosting White Mustards (*Sinapis alba*) Growth and Cadmium Uptake from Contaminated Soil. *ACS Omega* **2026**, *11*, 3738–3753.
33. Paulino, A.G.; da Cunha, A.J.; Alfaya, R.V.D.; et al. Chemically Modified Natural Cotton Fiber: A Low-Cost Biosorbent for the Removal of Cu(II), Zn(II), Cd(II), and Pb(II) from Natural Water. *Desalin. Water Treat.* **2014**, *52*, 4223–4233.
34. Dey, P.; Mahapatra, B.S.; Juyal, V.K.; et al. Flax Processing Waste—A Low-Cost, Potential Biosorbent for Treatment of Heavy Metal, Dye and Organic Matter Contaminated Industrial Wastewater. *Ind. Crops Prod.* **2021**, *174*, 114195.
35. Moyo, M.; Guyo, U.; Mawenyiyo, G.; et al. Marula Seed Husk (*Sclerocarya birrea*) Biomass as a Low Cost Biosorbent for Removal of Pb(II) and Cu(II) from Aqueous Solution. *J. Ind. Eng. Chem.* **2015**, *27*, 126–132.
36. Chen, Y.; Wang, J. Preparation and Characterization of Magnetic Chitosan Nanoparticles and Its Application for Cu(II) Removal. *Chem. Eng. J.* **2011**, *168*, 286–292.
37. Zhu, Y.; Hu, J.; Wang, J.; et al. Competitive Adsorption of Pb(II), Cu(II) and Zn(II) onto Xanthate-Modified Magnetic Chitosan. *J. Hazard. Mater.* **2012**, *221–222*, 155–161.
38. Kajelou, M.; Alem, A.; Mazghich, S.; et al. Competitive and Non-Competitive Zinc, Copper and Lead Biosorption from Aqueous Solutions onto Flax Fibers. *Chemosphere* **2020**, *260*, 127505.
39. Ben Amar, M.; Mallek, M.; Valverde, A.; et al. Competitive Heavy Metal Adsorption on Pinecone Shells: Mathematical Modelling of Fixed-Bed Column and Surface Interaction Insights. *Sci. Total Environ.* **2024**, *917*, 170398.
40. Mongiovi, C.; Lacalamita, D.; Morin-Crini, N.; et al. Use of Chenevotte, a Valuable Co-Product of Industrial Hemp Fiber, as Adsorbent for Copper Ions: Kinetic Studies and Modeling. *Arabian J. Chem.* **2022**, *15*, 103742.
41. Sehovic, E.; Memic, M.; Sulejmanovic, J.; et al. Thermodynamic Valorisation of Lignocellulosic Biomass Green Sorbents for Toxic Pollutants Removal. *Chemosphere* **2022**, *307*, 135737.
42. Abid, O.; Ahmed, E.; Shehzad, H.; et al. Competitive Recovery of Copper Ions Using Ethyl Acetoacetate Modified Chitosan/Organo-Functionalized Alginate Hydrogel Beads: Kinetics and Isothermal Sorption Studies. *Colloids Surf. A Physicochem. Eng. Asp.* **2023**, *675*, 132019.
43. Hong, H.J.; Ryu, J. Synthesis of Copper Nanoparticles from Cu^{2+}-Spiked Wastewater via Adsorptive Separation and Subsequent Chemical Reduction. *Nanomaterials* **2021**, *11*, 2051.
44. Iwuozor, K.O.; Oyekunle, I.P.; Oladunjoye, I.L.; et al. A Review on the Mitigation of Heavy Metals from Aqueous Solution Using Sugarcane Bagasse. *Sugar Tech* **2022**, *24*, 1167–1185.
45. Negi, A.; Joshi, S.; Joshi, S.K.; et al. Biosorption of Zinc on Functionally Activated *Lantana camara* Leaves: Equilibrium, Kinetic, and Thermodynamic Studies. *Biomass Convers. Biorefin.* **2025**, *15*, 24117–24134.
46. Ustun-Odabasi, S. Utilizing Sustainable Hemp Biomass as an Eco-Friendly for Potentially Toxic Elements Removal from Water. *Mater. Res. Express* **2024**, *11*, 025104.
47. Dhouibi, N.; Binous, H.; Dhaouadi, H.; et al. Hydrodistillation Residues of *Centaurea nicaeensis* Plant for Copper and Zinc Ions Removal: Novel Concept for Waste Re-Use. *J. Clean. Prod.* **2020**, *261*, 121106.
48. Bulgariu, L.; Fertu, D.I.; Cara, I.G.; et al. Efficacy of Alkaline-Treated Soy Waste Biomass for the Removal of Heavy-Metal Ions and Opportunities for Their Recovery. *Materials* **2021**, *14*, 7413.
49. Yalcin, M.S.; Ozdemir, S.; Kilinc, E.; et al. A Novel Magnetized Bio-Solid Phase Extractor for the Preconcentrations of Hg(II), Ni(II) and Zn(II) from Foods. *J. Food Compos. Anal.* **2024**, *134*, 106561.
50. Dong, J.; Sun, C.; Wang, Y.; et al. Adsorption characteristics of heavy metal ions from aqueous solution by fermented stalk. *Sci. Technol. Rev.* **2017**, *35*, 80–85.
51. Wang, Q.; Wang, Y.; Tang, J.; et al. New Insights into the Interactions between Pb(II) and Fruit Waste Biosorbent. *Chemosphere* **2022**, *303*, 135048.

52. Chen, C.; Wang, J. Removal of Pb^{2+}, Ag^{+}, Cs^{+} and Sr^{2+} from Aqueous Solution by Brewery's Waste Biomass. *J. Hazard. Mater.* **2008**, *151*, 65–70.
53. Wang, J.; Zhan, X.; Ding, D.; et al. Biosorption of Lead(II) from Aqueous Solution by Fungal Biomass of *Aspergillus niger*. *J. Biotechnol.* **2001**, *87*, 273–277.
54. Al-Zawahreh, K.; Albadarin, A.B. Assessment of Compost as a Dual-Performance Bioadsorbent for Removing Heavy Metals and Textile Dyes: An Overview. *Environ. Monit. Assess.* **2025**, *197*, 854.
55. Ocinski, D.; Augustynovicz, J.; Wolowski, K.; et al. Natural Community of Macroalgae from Chromium-Contaminated Site for Effective Remediation of Cr(VI)-Containing Leachates. *Sci. Total Environ.* **2021**, *786*, 147501.
56. Brahmi, A.; Zaabar, A.; Maizia, R.; et al. Leaves-Derived Cellulose Biosorbent for Efficient Hexavalent Chromium Removal: Integrating Density Functional Theory with Response Surface Methodology Optimization. *J. Water Process Eng.* **2025**, *79*, 108854.